View metadata, citation and similar papers at core.ac.uk
brought to you by CORE
provided by Florence Research

Accepted Manuscript

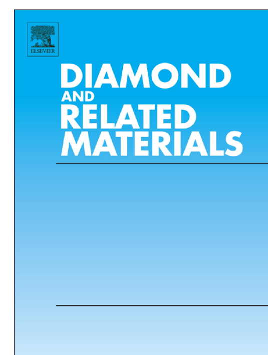

Optical properties of silicon-vacancy color centers in diamond created by ion implantation and post-annealing

Stefano Lagomarsino, Assegid M. Flatae, Silvio Sciortino, Federico Gorelli, Mario Santoro, Francesco Tantussi, Francesco De Angelis, Nicla Gelli, Francesco Taccetti, Lorenzo Giuntini, Mario Agio

PII: S0925-9635(17)30700-8
DOI: doi:10.1016/j.diamond.2018.03.010
Reference: DIAMAT 7050

To appear in: *Diamond & Related Materials*

Received date: 7 December 2017
Revised date: 8 March 2018
Accepted date: 12 March 2018

Please cite this article as: Stefano Lagomarsino, Assegid M. Flatae, Silvio Sciortino, Federico Gorelli, Mario Santoro, Francesco Tantussi, Francesco De Angelis, Nicla Gelli, Francesco Taccetti, Lorenzo Giuntini, Mario Agio , Optical properties of silicon-vacancy color centers in diamond created by ion implantation and post-annealing. The address for the corresponding author was captured as affiliation for all authors. Please check if appropriate. Diamat(2017), doi:10.1016/j.diamond.2018.03.010

This is a PDF file of an unedited manuscript that has been accepted for publication. As a service to our customers we are providing this early version of the manuscript. The manuscript will undergo copyediting, typesetting, and review of the resulting proof before it is published in its final form. Please note that during the production process errors may be discovered which could affect the content, and all legal disclaimers that apply to the journal pertain.

ACCEPTED MANUSCRIPT

Optical properties of silicon-vacancy color centers in diamond created by ion implantation and post-annealing

Authors

Stefano Lagomarsino[1,2], Assegid M. Flatae[1], Silvio Sciortino[2,3], Federico Gorelli[4,5], Mario Santoro[4,5], Francesco Tantussi[6], Francesco De Angelis[6], Nicla Gelli[2], Francesco Taccetti[2], Lorenzo Giuntini[2,3] and Mario Agio[1,4]

Affiliations:

[1]*Laboratory of Nano-Optics, University of Siegen, 57072 Siegen, Germany*
[2]*Istituto Nazionale di Fisica Nucleare, Sezione di Firenze, 50019 Sesto Fiorentino, Italy*
[3]*Department of Physics and Astrophysics, University of Florence, 50019 Sesto Fiorentino, Italy*
[4]*National Institute of Optics (INO), National Research Council (CNR), 50019 Sesto Fiorentino, Italy*
[5]*European Laboratory for Nonlinear Spectroscopy (LENS), 50019 Sesto Fiorentino, Italy*
[6]*Plasmon Nanotechnologies, Istituto Italiano di Tecnologia, 16163 Genoa, Italy*

Keywords: SiV centers, ion implantation, thermal activation, single-photon emitters

Abstract:

Silicon-vacancy (SiV) color centers have been created in diamond by ion implantation and post annealing at LABEC (Florence). A wide range of implantation depths (0-2.4 μm) and fluences (10^8-10^{15} cm^{-2}), along with a variety of substrates (single and poly-crystals) have been explored. The photoluminescence properties of the SiV centers have been studied at room temperature, including their single-photon emission characteristics. Single-photon emitters have been obtained at the lower-end of the implantation fluences range. They exhibit a short excited-state lifetime (~1 ns), a strong zero-phonon transition with a narrow linewidth (~1.6 nm) and a very small inhomogeneous broadening (0.015 nm), features that qualify them for application in quantum optical technologies. The activation yield of SiV centers has been assessed under different experimental conditions. It has been found to be independent of the implantation energy and in the range of 3% after thermal annealing.

1 Introduction

Color centers in diamond and other large band-gap semiconductors are promising candidates for the generation, storage and processing of quantum information[1,2,3,4,5], due to the combination of narrow spectral linewidths, high photon emission rates and optically addressable states with long coherence times. Compared to the current alternatives, such as trapped ions[6], nuclear spins[7], superconductive circuits[8] or semiconductor quantum dots[9], they have also the advantage of operating at room (or even higher[10]) temperature. A significant amount of work has been done in

ACCEPTED MANUSCRIPT

recent years on vacancy_related defects, mainly formed by an interstitial guest splitting two site vacancies along the 111 direction, like HeV[11], SV[12], GeV[13,14], SnV[15] and XeV[16] centers. In this regard, silicon-vacancy (SiV) color centers have recently shown the largest brightness for single-photon emission at room temperature[17] with a fluorescence emission concentrated in the zero-phonon line (ZPL) at 738 nm[18], with a room-temperature linewidth down to 0.7 nm [17]. SiV centers are also investigated in their orbital and electron spin coherence properties, as well as in techniques for coherent control of their quantum state, in view of possible applications in quantum information processing[19]. Moreover, available technologies for the fabrication of photonic waveguides and microcavities enable miniaturization and scalability of integrated optical devices[20,21,22,23].

We have recently developed a facility for the production of color centers in diamond, which is based on ion implantation in the pristine material followed by thermal activation of the centers in a high vacuum furnace[24]. Implantations take place at LABEC, the LABoratory for Environmental and Cultural heritage of the Florence section of the Italian National Institute of Nuclear Physics (INFN). The implantation facility is based on a 3MV Tandem accelerator (High Voltage Engineering Europe) equipped with a HVEE 860 Negative Sputter Ion Source, which allows for the acceleration of most ion species in the range of energies 1.4-15 MeV, depending on the terminal voltage and the ion charge state. Properly calibrated metal foils permit, if necessary, to degrade the ion energy down to a few tens of keV. The facility employs a double electrostatic deflector set-up for the generation of pulses with a time length selectable from a few ns to some µs, and it allows implantations in a broad range of fluences, from 10^8 to 10^{15} cm^{-2}, over areas which vary from a few μm^2 to some mm^2, depending on the mask employed. Such flexibility is useful to explore a wide range of implantation depths and fluences. The facility is completed by a custom-designed furnace for the optical activation of the centers, which allows for the fast heating of irradiated samples up to 1200 °C in high-vacuum conditions. The annealing procedures are described in detail in Ref.[10], the implantation facility and procedures in Refs.[24,25]. Here, we report on the optical properties of SiV color centers obtained in single- and poly-crystalline diamond matrices grown by chemical vapor deposition (CVD). For the creation of color centers, we accelerate Si^{3+} ions in the 6-10 MeV energy range. Since we are interested in the fabrication of emitters placed at depths varying from a few micrometers up to the shallower layers (within 200 nm from the surface), which require ion energies down to tens of keV, we have employed energy degraders (2.3 µm-thick Al layers)[24]. In the following, a detailed description of the setup for the optical characterization of the SiV centers is presented, along with experiments performed on different kind of samples obtained by varying the implantation parameters. Implantations at relatively high fluences (>10^{11} cm^{-2}) have been performed in single- and poly-crystals, whereas for the demonstration of single-photon emission, implantations at low fluences (10^8 – 10^9 cm^{-2}) in single crystals have been preferred.

2. Observation of the luminescence of the implanted centers

ACCEPTED MANUSCRIPT

Different techniques have been employed to investigate the optical property of SiV centers created at different implantation fluences. For high densities (irradiation fluence $\geq 10^{11}$ cm^{-2}), the SiV centers have been excited by a 647 nm continuous wave (cw) laser (Ar/Kr ion laser Coherent Innova 301 Krypton Ion Laser System) and the emission spectrum has been collected using a low numerical aperture (NA) objective (Mitutoyo Plan Apo SL Infinity-Corrected Objective, 20X, 0.28 NA), with a long working distance (30 mm) in a homebuilt confocal microscope configuration. The luminescence spectra have been analyzed by means of a single monochromator (Princeton Acton, Acton sp-500i, 500 mm focal length, 300 lines/mm grating) equipped with a notch filter (to suppress the laser emission line), and a charge-coupled device (CCD) detector (Princeton Instruments Spec-10:100BR) cooled below -120 °C by means of a liquid nitrogen reservoir. The relatively long depth of field of the low-NA objective (about 15 μm in air, 2.4 times more in diamond due to the larger refractive index) has been utilized to compare the luminescence signals from SiV centers implanted at different depths. The transversal spatial resolution for spectral detection and imaging of the system is 2 μm. The spectral resolution of the spectrometer is 0.3 nm at the emission wavelength of the SiV center. Micrometric automated XY movement (Newport translation stages equipped with homemade motorized actuators based on stepping motors controlled by micro step Pollux boxes) allows the acquisition of the spectra in 2-dimensional matrices with resolution and repeatability of the order of 1 μm.

The optical characterization of single SiV centers has been carried out, using another home-made confocal microscope connected to a spectrometer and a Hanbury-Brown and Twiss (HBT) interferometer, to measure the second order intensity autocorrelation function, as shown in Fig. 1. For photoluminescence (PL) measurements the sample is excited by a 647 nm cw laser at a power < 1mW (Coherent, Innova 70, Ar/Kr ion hybrid) and the emission from the sample is collected via a cover-slip corrected oil-immersion microscope objective (Olympus, 60X, 1.42 NA, 0.15 mm working distance). The spectrometer (Horiba, T64000) is equipped with a CCD (Jobin Yvon, Synapse, front illuminated open electrode, 1024×256 pixels) that exhibits a quantum efficiency around 40–50% at the emission wavelength of the SiV centers. Imaging of single SiV centers is performed using a flippable reflecting mirror placed along the optical axis of the setup. After wide field laser illumination, the collected signal is sent to an electron multiplying CCD (EM-CCD) camera (Princeton Instruments, ProEM-HS: 512 BX3, back-illuminated EMCCD, more than 90% quantum efficiency at the emission wavelength of the SiV). For measuring the anti-bunching behavior of SiV centers, a HBT interferometer is used. The laser excites a SiV center and the PL from the sample is spectrally filtered to suppress the laser line. A 50/50 non-polarizing beam splitter sends the emitted photons to two avalanche photodiodes (APDs) (Micro Photon Devices, 50 cps dark count). These detectors are connected to the start-stop time-interval analyzer of a time-correlated single photon counter (TCSPC) (PicoQuant, PicoHarp 300) and the delay between the arrival times of two emitted photons is repeatedly measured and histogrammed with picosecond time resolution. The excited-state lifetime of the SiV centers is measured using a pulsed diode laser (PicoQuant, PDL 800-D, LDH-D-C-660, 656 nm emission wavelength, 45 ps pulse width).

ACCEPTED MANUSCRIPT

ACCEPTED MANUSCRIPT

To avoid cross talk between the two APDs, a band pass filter is placed in front of them. The overall instrument response function (the resolution of the whole system) is less than 75 ps.

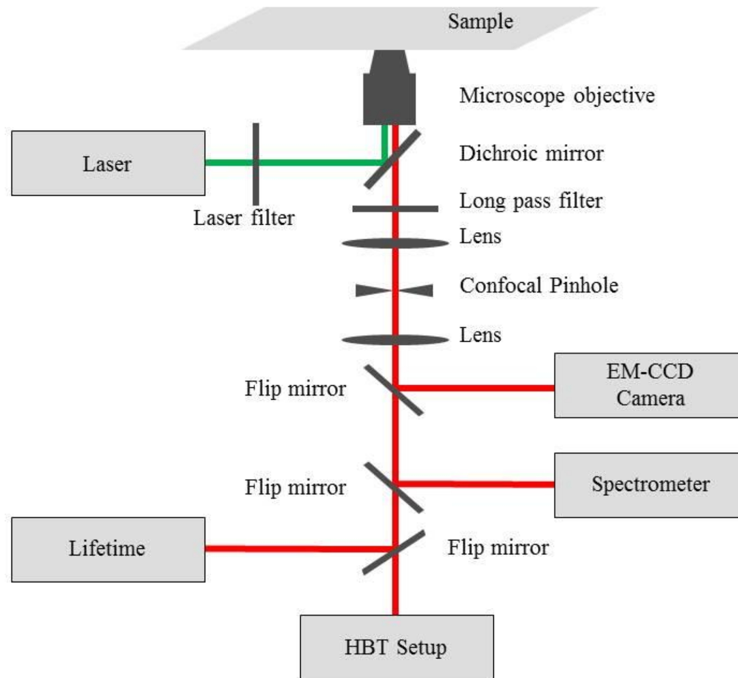

Figure 1. Scheme of the experimental setup for imaging, photoluminescence and excited state lifetime measurements. The HBT interferometer for measuring the anti-bunching behavior of single-photon sources is visible in the lower part of the picture.

3. Implantation experiments and results.

In order to implant Si ions in diamond at different depths, the accelerated ion energy (6 – 10 MeV) has been reduced to tens of keV by using 2.3 μm-thick Al foils. Placing 2, 1 or no Al foils leads to an implantation depth from 0 to about 2.4 μm. The actual depths, obtained at different beam energies with 0, 1 or 2 foils, are listed in Fig. 2(a). With 0 or 1 foil, nearly all the ions reach the diamond bulk and the reported depths refer to the Bragg peak position. The distribution widths, also specified in the figure, are larger for ions passing through the foil, due to the roughness of the foil itself. With 2 foils, the Bragg peak lies inside the Al foil and only a tail of the ion distribution reaches the diamond bulk, with a 1.2% and 30% transmission coefficient respectively for 8 and 10 MeV, as determined by SRIM simulations, where the roughness of the Al layers is taken into account. In these two cases, the ion distributions in diamond span a 0-100 nm and 0-400 nm range respectively. In our experiments, the fluence has been varied from 10^{8} to 10^{16} cm^{-2} on single-crystal

ACCEPTED

ACCEPTED MANUSCRIPT

and polycrystalline diamond substrates and the PL has been tested with and without thermal activation.

In the following we report on three cases because of their relevance in the investigation of the activation yield of SiV centers and its dependence on several process parameters:

1. Si ions implantation in single crystal diamond at constant fluence (3.2×10^{13} cm^{-2}), but different beam energies (6, 8 and 10 MeV) and 0, 1 or 2 Al foils as energy degraders. Energies and foil thicknesses have been selected in order to obtain approximately equally spaced end-of-range depths spanning from 0 to 2.4 μm. The luminescence spectrum has been measured before and after annealing at 1100 °C.
2. The same beam energies have been used for Si ion implantation on polycrystalline diamond, in order to assess possible correlations between the activation yield and the presence of crystal defects.
3. Implantations at low fluences (10^8–10^9 cm^{-2}) have been performed in order to observe single-photon emitters, their spectral characteristics, and directly measure the activation yield at low fluences.

3.1 High fluence implantations at different depths

A 5×5×0.5 mm^3 single-crystal diamond sample by E6®, covered with 0, 1 or 2 Al foils, as shown in Fig. 2(a), has been irradiated along three horizontal stripes at different energies (6, 8 and 10 MeV) in continuous mode operation. The exit slits of the beamline have been set at 2×0.5 mm^2, and the sample translated horizontally in front of the slits at a constant velocity, forward and backward, a number of times set in order to obtain an equal ion fluence in each zone. The irradiation time has been fixed according to the beam current measured before and after implantation by a Faraday cup, at each energy. As the ion currents is of the order of a few nA, some tens of cycles are sufficient in each case to obtain a fluence of 3.2×10^{13} cm^{-2}, with a 30% systematic error attributed to the Faraday cup measure. Figure 2(a) shows the appearance of the sample after irradiation but before annealing. Three dark strips ~0.5 mm wide (slightly larger due to the beam divergence) indicate the damage produced by the Si ions. No darkening is visible in the areas irradiated through the two foils by 6 and 8 MeV Si ions, because of the full stopping of the ions in aluminum in the former case and to the very small transmission coefficient (1.2%) in the latter.

ACCEPTED MANUSCRIPT

ACCEPTED MANUSCRIPT

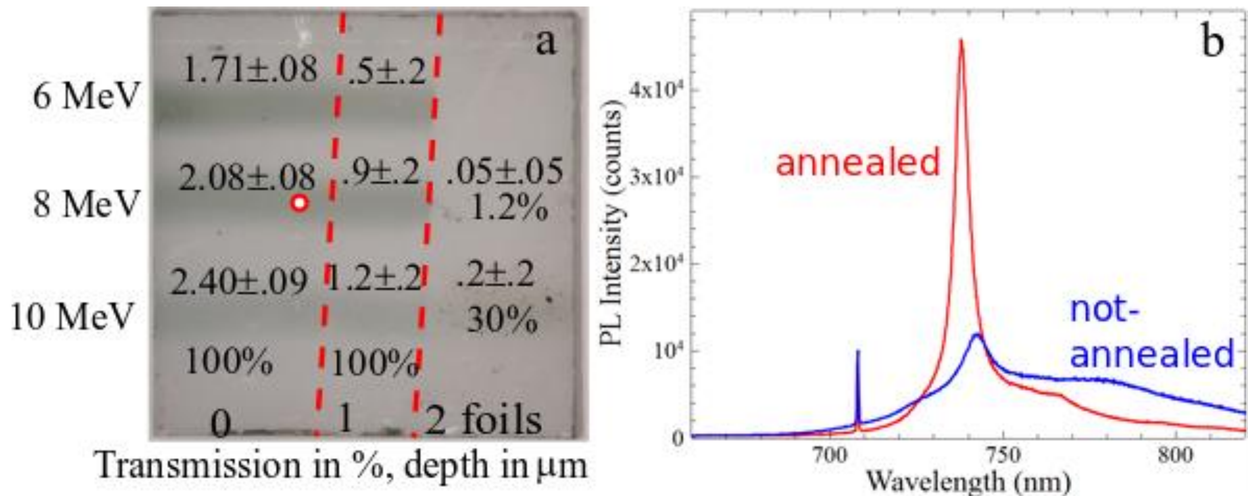

Figure 2 (a) Image of the sample taken after implantation, before annealing. The different stripes have been irradiated with ions of 6, 8 and 10 MeV energies (from top to bottom respectively) at 3.2×10^{13} cm^{-2} fluence. The red dashed lines delimit the areas irradiated through 0, 1 and 2 Al foils (left, middle, right respectively), resulting in the differently marked implantations. On the picture, the depths of the Bragg peaks are reported along with the dispersion of the ion distributions, calculated by SRIM simulations, taking into account 0.18 µm foil roughness. For 2 foils, the Bragg peak is inside the Al shield and the depths are the mean of the range covered by the tail of the ion distribution in diamond. (b) PL spectra, taken at the position marked by the red circle in Fig. 2(a), before (blue curve) and after (red curve) annealing at 1100 °C. Both spectra have been acquired with the same excitation power and integration time of 1 s. In both spectra the diamond Raman peak is clearly visible at 708 nm.

The spectral properties of the sample before and after annealing have been investigated using cw excitation. In Fig. 2(b), the typical spectra are shown, acquired by exciting the same area of the sample (8 MeV ion-energy, no Al shield and about 2.1 µm implantation depth) before (blue curve) and after annealing at 1100 ºC for 1 hour (red curve). Before annealing, the feature peaked at 742 nm is assignable to the zero-phonon line (ZPL) of the GR1 center, due to neutral vacancies generated in diamond by ion irradiation[26]. After annealing, the peak at 738 nm corresponds to the ZPL of the SiV color center. Thus, the pre-annealing spectra are dominated by the luminescence of the vacancies generated by ion damage (from about 700 to 1100 vacancies per ion, according to the ion energy and the thickness of the Al-degrader, as calculated by means of SRIM simulations[27,28]). On the other hand, after high temperature annealing, most of the Frenkel pairs have recombined, causing the disappearance of the 742 nm line, and the vacancies have been able to diffuse to form, together with the Si atoms dispersed in the lattice, the SiV complex responsible for the emission peaked at 738 nm. The attribution is also confirmed by the two false-color maps of the PL intensities at the ZPL, cleaned from background luminescence, before and after annealing, shown in Fig. 3.

ACCEPTED MANUSCRIPT

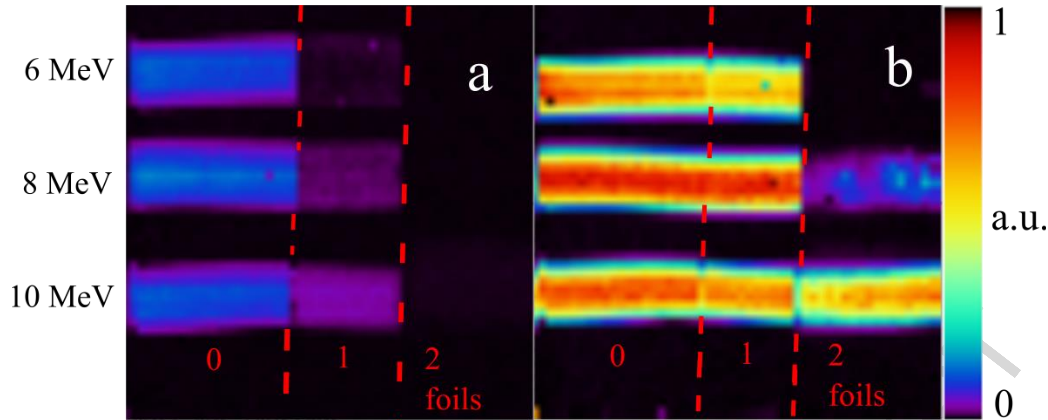

Figure 3 (a) ZPL luminescence intensity map of the GR1 centers in the sample of Fig. 2(a) after implantation and before annealing. (b) ZPL luminescent intensity map of the SiV centers after annealing at about 1100 °C for 1 hour.

Before annealing (Fig. 3(a)), the luminescence is directly correlated to the implantation depth, reflecting the growing overall number of vacancies generated per unit area. After annealing (Fig. 3(b)), all the areas in which the ions are transmitted with 100% of transmission ratio (those where the Bragg peak lies inside diamond at not less than 150 nm depth) show approximately the same PL intensity (within a max variation ascribable to the uncertainty in the overall ion fluence). Constant intensity reflects the same implantation fluence, assessing the independence of the activation yield on the implantation depth.

Since a direct counting of the centers is hampered by their high density, we have evaluated their surface concentration (thus the activation yield, by comparison with fluence) by measuring the ratio of the integrated PL and the diamond Raman line intensity. To this aim, as accounted for in the Appendix, the Raman cross section of diamond [29] has to be known, along with the characteristics of the focalized beam and some parameters concerning the photophysics of the SiV centers, namely the excited-state lifetime (see Sec. 3.3), the quantum yield and the saturation value of the laser power, previously measured under the same experimental conditions on centers implanted on the rear side of the same sample[10]. Due to the many parameters involved in the calculation, an uncertainty of 30% in the absolute value of the SiV centers density has to be considered.

In the areas where a uniform implantation fluence (3.2×10^{13} cm^{-2}) is obtained, an activation yield of 0.7% is measured with variations of the order of 13%, which are not correlated with the implantation depth, but rather with the long-term fluctuations in beam intensity, evaluated in a maximum of 30%. In the areas implanted through 2 Al foils, having respectively 30% and 1.2% of transmission ratio for 10 and 8 MeV ions (calculated by SRIM simulations), the yield was 2% and 6% respectively. Table 1 reports the measured activation yields compared with the implantation fluences.

ACCEPTED MANUSCRIPT

ACCEPTED MANUSCRIPT

Implantation fluence	3.2×10^{13} cm^{-2}	9.6×10^{12} cm^{-2}	3.8×10^{11} cm^{-2}
Activation yield (±30%)	0.7%	2%	6%

Tab 1. Activation yield of the SiV color centers as a function of the implantation fluence for the single-crystal sample.

In principle, the increased activation yield observed for decreasing fluence could depend on the decreasing implantation depth, but Schröder et al.[30], in a study performed at low energies (10-100 keV, thus with 20-70 nm Bragg peak depth) in the 10^{12} to 10^{14} cm^{-2} fluence range, observed a substiantial independence of the yield on the implantation depth in the first tens of nm, revealing a remarkable increase with decreasing fluences, down to 10^{12} cm^{-2}. Our study corroborates these conclusions extending the implantation depths up to a few microns and confirming a further increase of the yield down to the 10^{11} cm^{-2} fluence range.
The decrease of the yield for increasing fluences could be understood as a consequence of the presence of inactivated Si bystanders, altering the structure of the defect and possibly inhibiting the photon emission, e.g. by providing alternative de-excitation channels.
The independence of the activation yield on the implantation depth is not shared by other color centers, like the nitrogen-vacancy (NV), which show a remarkable decrease of the yield with decreasing implantation energies[31].

3.2 High fluence implantation of a polycrystalline sample

A polycrystalline diamond sample of detector grade quality by E6® has been implanted at 9 MeV energy in four different areas at 5.6×10^{13} cm^{-2}, 1.1×10^{13} cm^{-2}, 2.3×10^{12} cm^{-2} and 3.7×10^{11} cm^{-2} fluence, and then annealed at about 1100 °C for 1 hour. An estimate of the activation yield has been performed on the measured spectra as done for the single crystal described in Sec. 3.1, complicated by the random orientation of the diamond micro-grains. Assumed a completely random orientation, an average Raman cross-section $\frac{22}{15}$ of that found for a 100 crystal orientation - can be calculated (see Appendix for details). With this assumption, the yields in Tab. 2 have been evaluated for the four different fluences.

Implantation fluence	5.6×10^{13} cm^{-2}	1.1×10^{13} cm^{-2}	2.3×10^{12} cm^{-2}	3.7×10^{11} cm^{-2}
Activation yield (±30%)	0.5%	0.7%	1%	2.5%

Tab 2. Activation yield of the SiV color centers as a function of the implantation fluence for the polycrystalline sample.

A significant difference in the activation yield at the fluence in the range of 10^{12} cm^{-2} and below can be argued by comparison of Tab. 1 and Tab. 2. We believe this discrepancy at relatively low fluences to be related to the different nature and distribution of intrinsic structural defects in single-

ACCEPTED MANUSCRIPT

and poly-crystal diamond, supposedly sites of preferential activation of SiV centers. In single crystals the prevalent structural defects are dislocations randomly distributed, in poly-crystals grain boundaries present a characteristic distribution, whose cross section on the surface is roughly polygonal.

As a matter of fact, a detailed study on a limited surface of 120×120 μm^2 implanted at the lower fluence, revealed that the 738 nm luminescence is higher along the boundaries between polygonal domains. Figure 4(a) shows two spectra taken respectively on one of these boundaries and in a neighbor position, inside one domain.

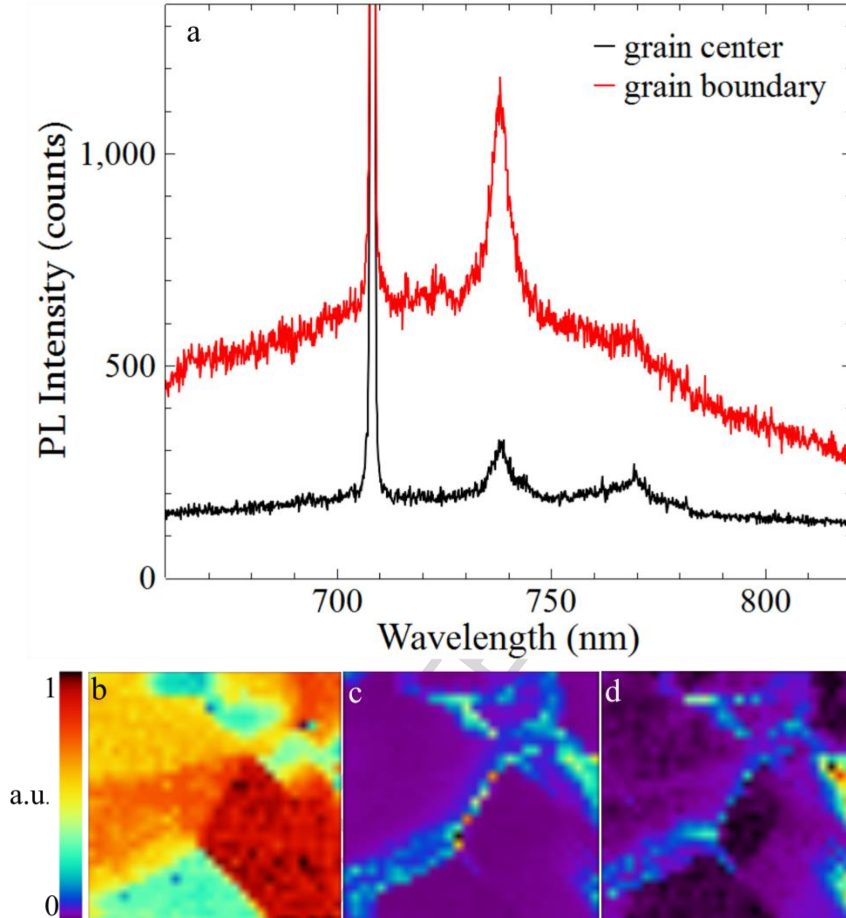

Figure 4 (a) PL spectra of the polycrystalline sample, respectively at the boundary between two domains (red curve) and inside one domain (black curve). The difference both in the SiV ZPL intensity signal and in the background luminescence is apparent. The 708 nm Raman line of diamond is included in the two spectra (intensity out of the scale of the plot). (b-c-d) Three maps of a same 120×120 μm^2 area. (b) Raman line intensity, on a scale ranging over a factor 2; the different intensities of the Raman signals from diverse diamond grains is apparent. (c) Luminescence background in the spectral window of SiV ZPL, evaluated as the average value of the signals at the two tails of the ZPL. (d) Integrated PL of the SiV ZPL, depurated from the background.

Figures 4(b)-4(d) show three maps of the same 120×120 μm^2 area. The first one represents the intensity of the diamond Raman line, which varies over a factor of two in the studied region. The picture shows that this variation is mainly related to the crystal orientation of the grains.

ACCEPTED MANUSCRIPT

Furthermore, it is apparent that the Raman line intensity varies from grain to grain, whose size is in the range from tens to a hundred of microns. The second map shows the background luminescence, arguably related to defects, which appear to be distributed along grain boundaries, as expected. The third map shows the spatial distribution of the SiV ZPL intensity, isolated from the background contribution (which has been obtained by subtracting a value corresponding to the average of the two tails). The close correlation between the density of the activated SiV centers and the grain boundaries is evident. The ratio 4:1 between the activation yield along the grain boundary and that in the grain center suggested by the two spectra of Fig. 4 (a) seems to be quite typical. The analysis shows that the activation of the SiV centers is much more probable where the native defects concentration is higher. This is reasonable as long as the center activation depends on the formation of complexes composed by a Si atom and a vacancy[32].

3.3 Low fluence implantation for single-photon sources

To demonstrate the potential of the technique for the fabrication of SiV-based single-photon sources, a CVD single-crystal diamond sample has been chosen. The ions have been implanted with fluences in the range of 10^8 - 10^9 cm^{-2} at depths ranging from a few tens of nm (8-9 MeV energies with 2 Al shields) to about 2 μm (10 MeV without shields). The samples have been annealed at 1000-1150 °C for 1 hour.

Figures 5(a) and (b) depict the wide-field fluorescence images of two areas implanted with 9 MeV ions through 2 Al foils at a fluence of 10^9 cm^{-2} and 10^8 cm^{-2} respectively (to the net of the ions stopped in aluminum), corresponding to an implantation depth of a few tens of nm.

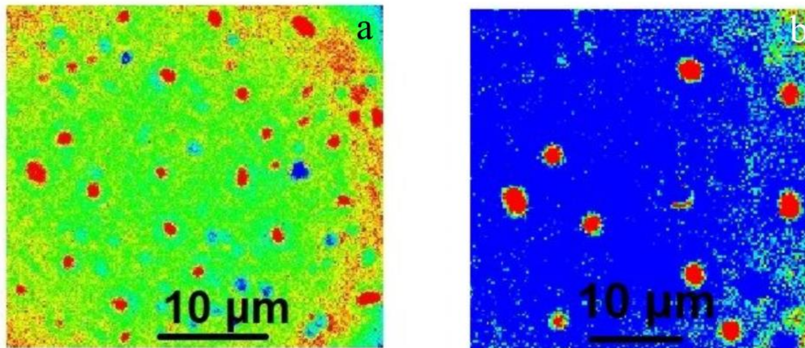

Figure 5. Wide-field fluorescence images of single SiV centers in diamond implanted at a fluence of 10^9 cm^{-2} (a) and 10^8 cm^{-2} (b).

The photon statistics and the intensity autocorrelation (second order correlation function) $g^{(2)}(\tau)$ have been measured for selected bright spots under confocal illumination and detection. The "stop" channel of the TCSPC is delayed by 100 ns in order to visualize negative correlations. A single-photon source cannot emit two photons at the same time. This is manifested by an intensity dip of the autocorrelation (see Fig. 6(a)) at a zero time-delay, when excited by a cw laser. Since $g^{(2)}(0)$ cannot be exactly zero, due to electronic and photonic noises, the value commonly accepted to

ACCEPTED MANUSCRIPT

define a single-photon emitter is $g^{(2)}(0) < 0.5$. Figure 6(a) shows that the PL of a single SiV center exhibits $g^{(2)}(0) = 0.27$. With pulsed laser excitation (at a repetition rate of 50 MHz), the photon detection events are spaced by the pulse period. A missing peak at zero-time delay confirms the emission from a single-photon source (see Fig. 6(b)).

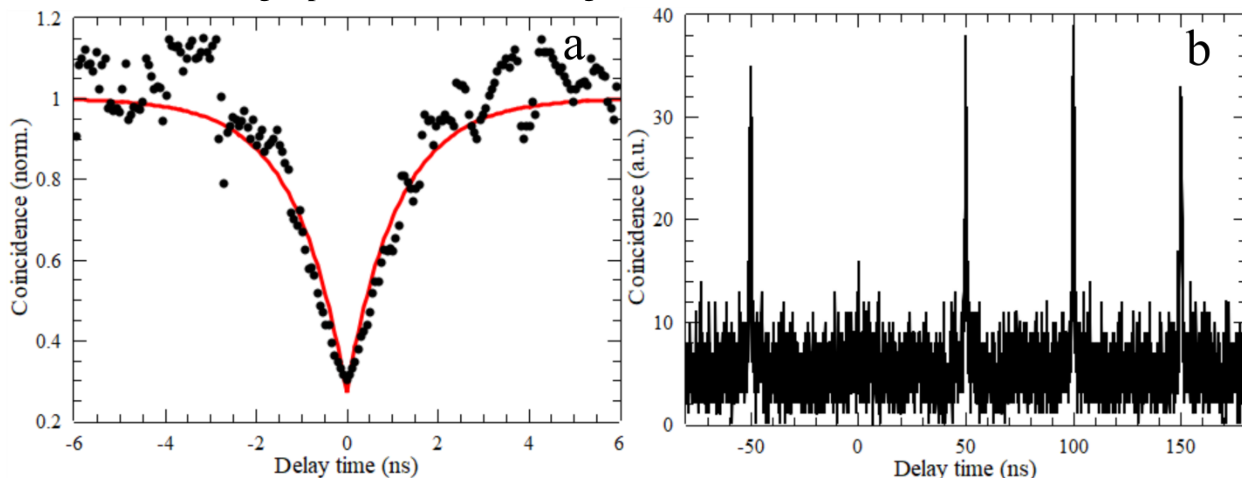

Figure 6 Intensity autocorrelation measurements using cw (a) and pulsed excitation (b) prove the single-photon characteristics of the SiV center. The red curve in (a) is a fit to the experimental data.

Nearly half of the emitters shown in Fig. 5(b) do not show anti-bunching behavior, indicating the presence of two or more emitting centers closer than the spatial resolution of the optical system. This can be hardly attributed to chance; in fact, although the implanted ion density goes from 1 to 10 per μm^2 in these samples, the activation yield is only a few percent, with an expected average distance between activated centers around 10 μm. A 50% frequency of multiple emitting centers is only conceivable if some mechanism of clustering is at work, for instance, if activation takes place preferentially at certain sites around which the formation of a SiV center could be energetically favored. In poly-crystals, grain boundaries have been proved to act as such preferential sites, in single crystals dislocations, the only extended defect ubiquitously distributed, are possible candidates to explain the observed high density of multiple centers. This point is still to be clarified and is currently under investigation.

The individual spectra of all single-emitters show an intense and narrow ZPL-emission centered at 738 nm with weak sidebands (statistical average over 10 centers (738.1±0.015) nm), with a linewidth of about 1.6 nm (statistical average over 10 centers (1.59±0.01) nm). Such a level of inhomogeneous broadening, amounting to about 8 GHz (but depending on the strain state of the substrate), would facilitate the search for a couple of centers whose difference in emission frequency lies within the ZPL transition at 4 K, enabling quantum interference between single photons from separated sources[5, 33]. On the other hand, coupling the SiV center with nanoresonators[23,34] could increase the emission rate by orders of magnitude and make the emission of indistinguishable photons from two different quantum emitters at room temperature possible. Figure 7(a) shows the spectrum of one of the SiV centers, with emission centered at 738.1 nm and a linewidth of 1.58 nm. The strength of the ZPL line is determined by the so-called Debye-Waller

ACCEPTED MANUSCRIPT

(DW) factor (the ratio of the ZPL intensity to the overall emission), which is found to be more than 0.94. This makes these SiV centers ideal for many applications, where a bright and narrowband emission not affected by inhomogeneous broadening is needed. Another important parameter of a single-photon source is the maximum photon count rate I_∞. Figure 7(b) shows the count rate I of one SiV center as a function of excitation power P. The measured data have been fitted using $I = I_\infty/(1+P_{sat}/P)$, where P_{sat} is the saturation power. Taking into consideration the intensity dependent background florescence on the diamond host material, a maximum count rate $I_\infty = (3.80\pm0.03)\times10^3$ count/s and a saturation power $P_{sat}= (117\pm4)$ μW have been found. These values do not take into account the outcoupling efficiency, which for a dipole source in bulk diamond is of the order of a few percent, optical losses in the setup and the efficiency of the APDs. Moreover, the saturation curve in Fig. 7(b) has been measured for an arbitrary SiV center (unknown dipole orientation). Further investigations on the dipole orientation, outcoupling and detection efficiencies, saturation curves and intensity dependent de-shelving can eventually determine the center quantum efficiency[35].

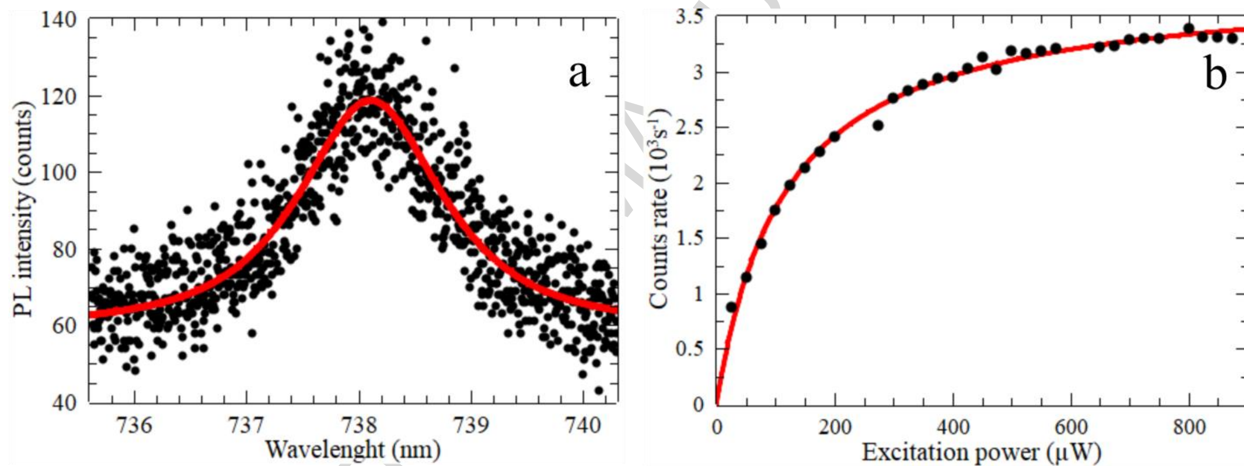

Figure 7 (a) Emission spectrum of a SiV center. (b) PL saturation curve of a SiV centre.

Another interesting feature of the SiV color centers is the short excited-state lifetime, which is about 1 ns (statistical average over 10 centers (1.03±0.06) ns), as shown in Fig. 8.

ACCEPTED MANUSCRIPT

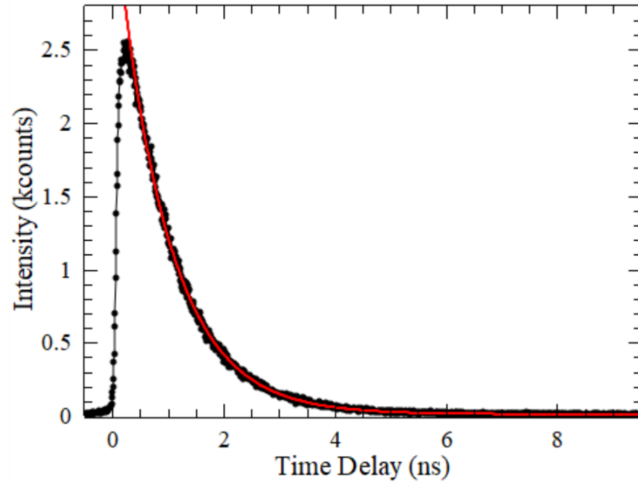

Figure 8. Fluorescence lifetime measurement of a SiV center exhibiting an excited-state lifetime of 0.93 ns.

In general, all the investigated single SiV centers exhibit almost identical optical properties (position of the ZPL, spectral linewidth and excited-state lifetime), which makes the SiV center a promising single-photon source, especially when high emission rates of indistinguishable photons are required.

Finally, counting the luminescence bright spots in wide-field images permits an estimation of the activation efficiency of the implantation process. The number of Si ions implanted in diamond per unit area is of the order of 1 or 10 μm^{-2} for fluences of 10^8 cm^{-2} or 10^9 cm^{-2}, respectively. A direct counting of the bright spots in images like those of Fig. 5 shows a degrading centers density from the center to the peripheral area of the implantation. For the implantations performed at 10^9 cm^{-2} direct counting is difficult because in the higher density areas most centers cannot be resolved. On the other hand, the maximum densities for the 10^8 cm^{-2} implantations are 25±5 centers in a 1000 μm^2 area, suggesting an activation yield of (2.5±0.5)%. This value has to be corrected taking into account the occurrence of multiple centers, in the just mentioned ratio of 50%. As a consequence, the activation yield could be about (3.8±0.8)%. This value is not far from those measured by Schröder et al., and it is consistent with that measured for the lowest implantation fluences in the single crystal with the method of the ratio between the SiV and the diamond Raman line intensity (see Sec. 3.1), despite the large experimental error.

4. Conclusions

The implantation facility at the electrostatic deflector (DEFEL) line of the 3 MeV Tandetron accelerator of the LABEC laboratory in Florence (Italy) has been exploited for the creation of SiV centers in different kinds of diamond samples (single-crystal and poly-crystalline), over a wide range of implantation fluences (10^8–10^{15} cm^{-2}) and implantation depths (0–2.4 μm). In all these cases, the thermal activation yield of the color centers has been assessed after proper thermal annealing. It has been found that native defects (e.g. grain boundaries in polycrystalline materials)

ACCEPTED MANUSCRIPT

enhance the thermal activation of SiV centers, while the implantation depth is quite irrelevant, differently from other implanted color centers like NV[31]. In the low fluence regime, the activation yield also seems to be independent on the implantation fluence.

The single-photon emission characteristics of the SiV centers have been verified using PL and time-resolved spectroscopy. Most of the fluorescence signal is concentrated in the narrow ZPL at 738 nm, with a room temperature linewidth down to 1.6 nm. This is due to a very large Debye-Waller factor, which reaches 0.94. Moreover, the SiV centers exhibit a very small inhomogeneous broadening (~ 0.015 nm around the ZPL) and a short excited-state lifetime (~ 1 ns). These features make the SiV centers ideal candidates for many applications based on single-photon emitters. In particular, the spectral quality and reproducibility of the optical properties make these solid-state emitters promising for the production of indistinguishable photons from separated centers.

Prime novelty statement

We have assessed the correlation between the activation yield of implanted SiV centers and the native defects concentration in polycrystalline diamond. We have applied an innovative method for the measurement of the activation yield for high density implantations based on comparison between the SiV and the diamond Raman line intensity. We have found that, differently from other implanted color centers, the activation yield of the SiV is independent on the implantation energy. We found that SiV centers implanted at LABEC exhibit spectral quality and reproducibility suitable for quantum applications, for instance for the scalable production of bright single photon sources.

Acknowledgments

Financial support from the EC Seventh Framework Programme (248855), the Helmoltz Association (283286), the University of Siegen and Istituto Italiano di Tecnologia is gratefully acknowledged. The authors warmly thank INFN-CHNet, the network of laboratories of the INFN for cultural heritage, for support and precious contributions in terms of instrumentation and personnel. This article is based upon work from COST Action MP1403 "Nanoscale Quantum Optics," supported by COST (European Cooperation in Science and Technology). We gratefully thank also Nicole Fabbri, Costanza Toninelli and Silvia Orlanducci for helpful discussions.

Appendix: Evaluation of the SiV surface density by comparison of the SiV luminescence and the Raman line intensity

The number of SiV centers activated per unit area n_{SiV} can be evaluated measuring the ratio ρ between their integrated luminosity and that of the diamond Raman line. This can be assumed to be comparable to the ratio between the number of photons $\frac{dN_{SiV}}{dt}$, emitted in the backward direction per unit solid angle by the SiV centers in the unit time, and $\frac{dN_R}{dt}$, the number of those backscattered by diamond due to Raman

ACCEPTED MANUSCRIPT

effect. Both these photon fluxes comes from the same volume V, equaling the cross section of the laser beam waist S times $nd/2$, the product of half the depth of field d and the refraction index n of diamond (n=2.41). The two ratios are assumed equal providing that the transfer function of the optical system is weakly dependent on the wavelength and that the collection efficiencies for the fluorescence and Raman signals are the same.

Now

$$\frac{dN_R}{dt} = \frac{\bar{E}}{h_{Plank}\nu_L} \cdot S \cdot \frac{nd}{2} \cdot n_C \cdot \sigma_{R.}$$

Where σ_R is the Raman differential cross section in the backward direction, n_C is the density of carbon atoms (1.76×10^{23} cm^{-3}), ν_L is the frequency of the laser photons (647 nm in our case) and $\bar{E}=P/S$ is the average illuminance in the volume V, given by the ratio between the laser power transmitted in diamond and the laser beam cross section S (used values are reported below).

Thus, we have

$$\frac{dN_{SiV}}{dt} = \varrho \cdot \frac{P}{h_{Plank}\nu_L} \cdot \frac{nd}{2} \cdot n_C \cdot \sigma_{R.}$$

Now, if the emission of the centers is assumed isotropic, due to their random orientation in the diamond lattice, $\frac{dN_{SiV}}{dt}$ is bound to the density of the excited SiV centers n^*_{SiV} by the equation

$$\frac{dN_{SiV}}{dt} = \frac{1}{4\pi}\frac{\eta}{\tau} n^*_{SiV} \cdot S,$$

Where η is the quantum yield and τ is the lifetime of the excited level. On the other hand, $n_{SiV}{}^*$ depends on the power level P according to

$$n^*_{SiV} = \frac{P}{P + P_{sat}} n_{SiV}$$

So that we find

$$n_{SiV} = \varrho \cdot \frac{\tau}{\eta} \cdot \frac{(P + P_{sat})/S}{h\nu_L} \cdot \frac{nd}{2} \cdot n_C \cdot 4\pi\sigma_{R.}$$

In our measurements, we have τ=1.1 ns, $P\cong36$ mW, P_{sat}=75 mW, $S=\pi10^{-8}$cm^2, d=20µm. η is evaluated as 30% for SiV centers in diamond bulk. The quantity $4\pi\sigma_R$ has been measured in backscattering configuration for a 111 oriented crystal and equals, at λ_i= 785 nm of excitation wavelength (λ_s= 877 nm scattered wavelength), 2.7×10^{-29} cm^2 per carbon atom[29]. Our crystals are 100 oriented, so the Raman cross section reduces to 3/5 of the value relative to the 111 direction of propagation.

ACCEPTED MANUSCRIPT

The ratio of the two Raman cross sections for unpolarized scattered light has been calculated taking into account $\sigma_R = \sum_{ij}(e^I \alpha_i \, e_j^R)^2$ where α_i is the Raman polarizability tensor relative to the *i*-th irreducible representation of the punctual group of the crystal, e^I is the polarization vector of the incident light and e^R_j are the two orthogonal polarization vectors of the scattered light. For diamond the non-null tensors referred to the 100, 010 and 001 directions are[36] $\begin{pmatrix} 0 & 0 & 0 \\ 0 & 0 & d \\ 0 & d & 0 \end{pmatrix}; \begin{pmatrix} 0 & 0 & d \\ 0 & 0 & 0 \\ d & 0 & 0 \end{pmatrix}; \begin{pmatrix} 0 & d & 0 \\ d & 0 & 0 \\ 0 & 0 & 0 \end{pmatrix}$

The excitation wavelength is λ'_i= 647 nm (λ'_s =708 nm scattered light), so the Raman cross section per carbon atom in our experimental conditions can be evaluated as

$$4\pi\sigma_R^{(100)}(\lambda_i') = \frac{3}{5} \cdot \frac{{\lambda_s}^3 \lambda_i}{{\lambda_s}'^3 {\lambda_i}'} 4\pi\sigma_R^{(111)}(\lambda_i) = 3.7 \cdot 10^{-29} cm^2$$

Once n_{SiV} has been evaluated, the activation yield is promptly calculated as ϕ / n_{SiV}, where ϕ is the implantation fluence.

In the case of the polycrystalline sample, the Raman cross section $\sigma R(\theta,\phi)$ for a random orientation of the crystal has been calculated and the ratio $\int \sigma_R(\theta, \varphi) cos\theta d\theta d\varphi / \sigma_R(< 100 >) = \frac{22}{15}$ has been taken into account.

ACCEPTED MANUSCRIPT

ACCEPTED MANUSCRIPT

[1] C. Kurtsiefer, S. Mayer, P. Zarda & H. Weinfurter *Stable solid-state source of single photons*. Phys. Rev. Lett. 85, 290–293 (2000)

[2] B.J.M. Hausmann, B. Shields, Q. Quan, P. Maletinsky, M. McCutcheon, J.T. Choy, T.M. Babinec, A. Kubanek, A. Yacoby, M.D. Lukin and M. Loncar, *Integrated Diamond Networks for Quantum Nanophotonics*. Nano Lett. 12, 1578 (2012)

[3] F. Fuchs, B. Stender, M. Trupke, D. Simin, J. Pflaum, V. Dyakonov & G.V. Astakhov. *Engineering near-infrared single-photon emitters with optically active spins in ultrapure silicon carbide*. Nat. Commun. 6, Article number: 7578 (2015)

[4] M. Widmann, S.Y. Lee, T. Rendler, N. Tien Son, H. Fedder, S. Paik, Li-Ping Yang, N. Zhao, S. Yang, I. Booker, A. Denisenko, M. Jamali, S.A. Momenzadeh, I. Gerhardt, T. Ohshima, A. Gali, E. Janzén and J. Wrachtrup. *Coherent control of single spins in silicon carbide at room temperature*. Nat. Mater. 14, 164–168 (2015).

[5] A. Sipahigil, K. D. Jahnke, L. J. Rogers, T. Teraji, J. Isoya, A. S. Zibrov, F. Jelezko and M. D. Lukin. *Indistinguishable Photons from Separated Silicon-Vacancy Centers in Diamond*. PRL 113, 113602 (2014)

[6] R. Blatt and D. Wineland. *Entangled states of trapped atomic ions*. Nature 453, 1008–15 (2008)

[7] L.M. Vandersypen, M. Steffen, G. Breyta, C.S. Yannoni, M.H. Sherwood and I.L. Chuang. *Experimental realization of Shor's quantum factoring algorithm using nuclear magnetic resonance*. Nature 414, 883–7 (2001)

[8] C. Rigetti, J.M. Gambetta, S. Poletto, B.L.T. Plourde, J.M. Chow, D. Córcoles, J.A. Smolin, S.T. Merkel, J.R. Rozen, G.A. Keefe, M.B. Rothwell, M.B. Ketchen and M. Steffen. *Superconducting qubit in a waveguide cavity with a coherence time approaching 0.1 ms.* Phys. Rev. B 86, 100506 (2012)

[9] D. Press, T.D. Ladd, B. Zhang and Y. Yamamoto. *Complete quantum control of a single quantum dot spin using ultrafast optical pulses*. Nature 456, 218–21 (2008).

[10] S. Lagomarsino, F. Gorelli, M. Santoro, N. Fabbri, A. Hajeb, S. Sciortino, L. Palla, C. Czelusniak, M. Massi, F. Taccetti, L. Giuntini, N. Gelli, D. Y. Fedyanin, F.S. Cataliotti, C. Toninelli and M. Agio. *Robust luminescence of the silicon-vacancy center in diamond at high temperatures*. AIP ADVANCES 5, 127117 (2015)

[11] J. Forneris, A. Tengattini, S. Ditalia Tchernij, F. Picollo, A. Battiato, P. Traina, P. Degiovanni, E. Moreva, G. Brida, V. Grilj, N. Skukan, M. Jakšić, M. Genovese, P. Olivero, *Creation and characterization of He-related color centers in diamond*, Journal of Luminescence, 179 (2016) 59-63

[12] G.D. Cheng, Q. Huang, Y.H. Shen, H.F. Huang, L. Yan, *Theory of sulfur-vacancy defect in diamond: a comparable NV−1 isoelectronic center*, Electron Optics 136 (2017) 151-156

[13] M. K. Bhaskar, D. D. Sukachev, A. Sipahigil, R. E. Evans, M. J. Burek, C. T. Nguyen, L. J. Rogers, P. Siyushev, M. H. Metsch, H. Park, F. Jelezko, M. Lončar, and M. D. Lukin. *Quantum Nonlinear Optics with a Germanium-Vacancy Color Center in a Nanoscale Diamond Waveguide*. Phys. Rev. Lett. 118, 223603 – Published 31 May 2017

[14] K.N. Boldyrev, B.N. Mavrin, P.S. Sherin, M.N.Popova, *Bright luminescence of diamonds with Ge-V centers*, Journal of Luminescence 193 (2018) 119-124

[15] T. Iwasaki, Y. Miyamoto, T. Taniguchi, P. Siyushev, M.H. Metsch, F. Jelezko and M. Hatano *Tin-Vacancy Quantum Emitters in Diamond.* Phys. Rev. Lett. 119, 253601 – Published 22 December 2017

[16] R. Sandstrom, L. Ke, A. Martin, Z.Wang, M. Kianinia, B. Green, W.-b. Gao, I. Aharonovich, *Optical properties of implanted Xe color centers in diamond*, Optics Communications 411 (2018) 182-186

[17] E. Neu, D. Steinmetz, J. Riedrich-Möller, S. Gsell, M. Fischer, M. Schreck, and C. Becher. *Single photon emission from silicon-vacancy colour centres in chemical vapour deposition nano-diamonds on iridium*. New J. Phys. 13, 025012 (2011)

[18] S. Pezzagna, D. Rogalla, D. Wildanger, J. Meijer and A. Zaitsev. *Creation and nature of optical centres in diamond for single-photon emission—overview and critical remarks.* New Journal of Physics 13(2011) 035024

ACCEPTED MANUSCRIPT

ACCEPTED MANUSCRIPT

[19] J.N. Becker, C. Becker. *Coherence Properties and Quantum Control of Silicon Vacancy Color Centers in Diamond*. Phys. Status Solidi A, 1700586 (2017)

[20] M.P. Hiscocks, K. Ganesan, B.C. Gibson, S.T. Huntington, F. Ladouceur and S. Prawer. *Diamond waveguides fabricated by reactive ion etching*. Optics Express, 16:19512, 2010.

[21] S. Lagomarsino, P. Olivero, F. Bosia, M. Vannoni, S. Calusi, L. Giuntini, M. Massi. *Evidence of light guiding in ion-implanted diamond*. Physical review letters. 105, (2010) 233903

[22] T.M. Babinec, B.J.M. Hausmann, M. Khan, Y. Zhang, J.R. Maze, P.R. Hemmer & M. Lončar. *A diamond nanowire single-photon source*. Nature Nanotechnology 5, 195 - 199 (2010)

[23] J. Riedrich-Möller, L. Kipfstuhl, C. Hepp, E. Neu, C. Pauly, F. Mücklich, A. Baur, M. Wandt, S. Wolff, M. Fischer, S. Gsell, M. Schreck & C. Becher. *One- and two-dimensional photonic crystal microcavities in single crystal diamond*. Nature Nanotechnology 7, 69–74 (2012)

[24] S. Lagomarsino, S. Sciortino, N. Gelli, A. M. Flatae, F. Gorelli, M. Santoro, M. Chiari, C. Czelusniak, M. Massi, F. Taccetti, M. Agio, and L. Giuntini. *The center for production of single-photon emitters at the electrostatic-deflector line of the Tandem Accelerator of LABEC (Florence)* Nuclear Instruments and Methods in Physics Research B 422 (2018) 31-40

[25] N. Taccetti, L. Giuntini, G. Casini, A.A. Stefanini, M. Chiari, M.E. Fedi, P.A. Mandò, *The pulsed beam facility at the 3 MV Van de Graaff accelerator in Florence: Overview and examples of applications*, Nuclear Instruments and Methods in Physics Research B 188 (2002) 255-260

[26] I. Kiflawi, A.T. Collins, K. Iakoubovskii and D. Fisher. *Electron irradiation and the formation of vacancy–interstitial pairs in diamond*. J. Phys.: Condens. Matter 19 (2007) 046216

[27] J.F. Ziegler, M.D. Ziegler, J.P. Biersack, *SRIM – The stopping and range of ions in matter (2010),* Nuclear Instruments and Methods in Physics Research B 268 (2010) 1818–1823

[28] http://www.srim.org

[29] R.L. Aggarwal, L.W. Farrar, S.K. Saikin , X. Andrade, A. Aspuru-Guzik, D.L. Polla. *Measurement of the absolute Raman cross section of the optical phonons in type Ia natural diamond*. Solid State Communications 152 (2012) 204–209

[30] T. Schröder, M. E. Trusheim, M. Walsh, L. Li, J. Zheng, M. Schukraft, A. Sipahigil, R. E. Evans, D.D. Sukachev, C.T. Nguyen, J.L. Pacheco, R.M. Camacho, E.S. Bielejec, M.D. Lukin & D. Englund. *Scalable focused ion beam creation of nearly lifetime-limited single quantum emitters in diamond nanostructures*. Nature Communications 8, (2017) 15376.

[31] S. Pezzagna, B. Naydenov, F. Jelezko, J. Wrachtrup and J. Meijer. *Creation efficiency of nitrogen-vacancy centres in diamond.* New Journal of Physics 12, 065017 (2010)

[32] U. F. S. D'Haenens-Johansson, A. M. Edmonds, B. L. Green, M. E. Newton, G. Davies, P. M. Martineau, R. U. A. Khan, and D. J. Twitchen. *Optical properties of the neutral silicon split-vacancy center in diamond*. Phys. Rev. B 84 (2011) 245208

[33] L.J. Rogers, K.D. Jahnke, T. Teraji, L. Marseglia, C. Müller, B. Naydenov, H. Schauffert, C. Kranz, J. Isoya, L.P. McGuinness & F. Jelezko. *Multiple intrinsically identical single-photon emitters in the solid state.* Nature Communications 5 (2014) 4739

[34] M. Agio. *Optical antennas as nanoscale resonators*. Nanoscale 4, 692 (2012)

[35] E. Neu, M. Agio and C. Becher. *Photophysics of single silicon vacancy centers in diamond: implications for single photon emission*. Optics Express 20 (18) 19956-19971 (2012)

[36] R. Loudon. *The Raman Effect in Crystals*. Advances in Physics. 13 (1964) 423-481

ACCEPTED MANUSCRIPT

ACCEPTED MANUSCRIPT

Graphical abstract

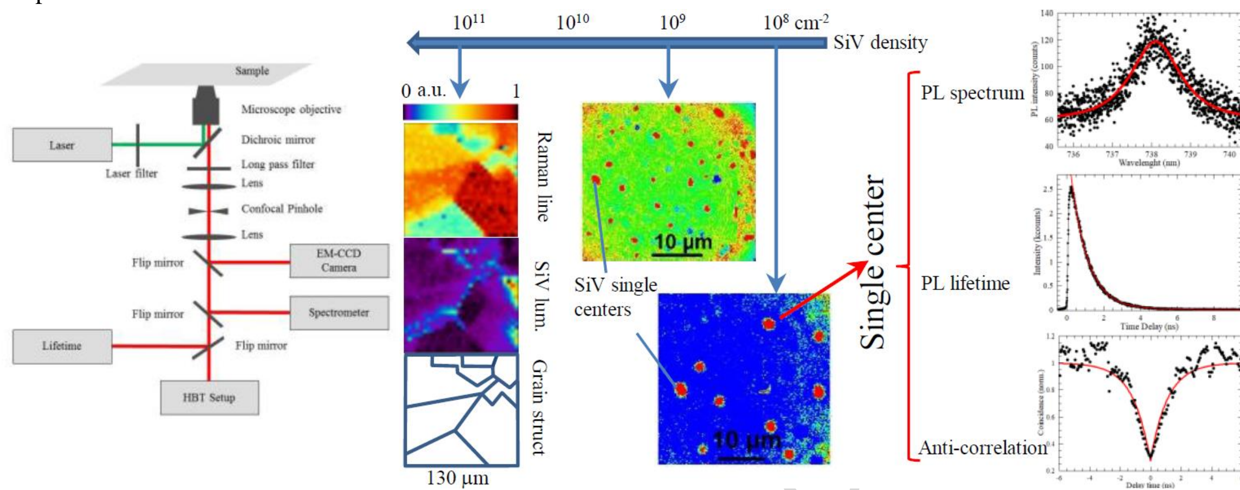

ACCEPTED MANUSCRIPT

ACCEPTED MANUSCRIPT

Optical properties of silicon-vacancy color centers in diamond created by ion implantation and post-annealing

Highlights:

- Single-photon SiV color centers created in diamond by ion implantation
- Excellent spectral quality and reproducibility
- Wide range of process parameters explored
- Activation yield independent on implantation energy
- Activation yield dependent on native defects concentration

ACCEPTED MANUSCRIPT